UNSTEADY AERODYNAMIC MODELING USING NEURO-FUZZY APPROACHES COMBINED WITH POD

M. Winter*, C. Breitsamter†
Institute of Aerodynamics and Fluid Mechanics, Technische Universität München
Boltzmannstr. 15, 85748 Garching, Germany

Abstract

In the present work, an efficient surrogate-based framework is developed for the prediction of motion-induced surface pressure fluctuations. The model construction is realized by performing forced-motion computational fluid dynamics (CFD) simulations, while the result is processed via the proper orthogonal decomposition (POD) to obtain the most relevant flow modes. Subsequently, a nonlinear system identification is carried out with respect to the applied excitation signal and the corresponding POD coefficients. For the input/output model identification task, a recurrent local linear neuro-fuzzy approach is employed in order to capture the linear and nonlinear characteristics of the dynamic system. Once the reduced-order model (ROM) is trained, it can substitute the flow solver within an aeroelastic simulation framework for a given configuration at a fixed set of free-stream conditions. For demonstration purposes, the ROM approach is applied to the LANN wing in transonic flow. Due to the characteristic lambda-shock system, the unsteady aerodynamic surface pressure distribution is dominated by nonlinear effects. Preliminary numerical investigations show a good correlation between the results obtained by the ROM methodology in comparison to the full-order CFD solution. In addition, the surrogate approach yields a significant speed-up regarding unsteady aerodynamic calculations, which is beneficial for aeroelastic applications, local load estimation, and multidisciplinary computations.

NOMENCLATURE

$\boldsymbol{A}$	=	time-averaged pressure coefficient for each surface element ($S \times 1$)
$\boldsymbol{B}$	=	POD coefficient matrix ($M \times N_{Trn}$)
$\boldsymbol{b}$	=	POD coefficient vector ($M \times 1$)
b_i	=	coefficient related to POD mode i
$\tilde{b}_i$	=	predicted POD coefficient (mode i)
$\boldsymbol{c}_i$	=	center vector of neuron i
C_L, C_M	=	lift and pitching moment coefficient
C_p	=	pressure coefficient ($= (p - p_\infty)/q_\infty$)
c_{ref}	=	reference chord length, m
f	=	oscillation frequency, Hz
k	=	time step
k_{red}	=	reduced frequency ($= 2\pi f \cdot c_{ref}/U_\infty$)
M	=	number of considered POD modes
Ma_∞	=	free-stream Mach number
m	=	maximum input delay
N_{LLM}	=	number of neurons
N_{Trn}	=	number of training samples
n	=	maximum output delay
p	=	dimension of input vector $\boldsymbol{u}_i$
p, p_∞	=	(free-stream) static pressure, N/m²
$\boldsymbol{q}$	=	vector of generalized coordinates
q_∞	=	free-stream dynamic pressure, N/m²
S	=	number of surface elements
T	=	nondimensional cycle period
t	=	time, s
$\boldsymbol{U}$	=	unitary matrix ($S \times S$), result of SVD
U_∞	=	free-stream velocity, m/s
$\boldsymbol{u}_i$	=	neural network input vector ($p \times 1$)
$u_{x,i}$	=	input vector element x related to $\tilde{b}_i$
$\boldsymbol{W}_i$	=	snapshot vector ($S \times 1$) at time i
$\widehat{\boldsymbol{W}}_i$	=	centered snapshot vector ($S \times 1$)
w_{xy}	=	linear model parameters (weights)
$\boldsymbol{Y}$	=	POD snapshot matrix ($S \times N_{Trn}$)
α	=	angle of attack, deg ($\alpha = \alpha_0 + \hat{\alpha}$)
α_0	=	mean angle of attack, deg
$\hat{\alpha}$	=	amplitude angle of attack, deg
Δt	=	dimensional time step size, s
$\Delta\tau$	=	nondimensional time step size
ε	=	user-defined threshold (POD)
ρ_∞	=	free-stream density, kg/m³
$\boldsymbol{\Sigma}$	=	matrix ($S \times N_{Trn}$) containing σ_i (SVD)
σ_i	=	singular value
σ_{xy}	=	basis function width
τ	=	nondimensional time
$\boldsymbol{\phi}_i$	=	POD mode i ($S \times 1$)
Ψ_i	=	validity function operator

1. INTRODUCTION

Unsteady aerodynamic phenomena and fluid-structure interaction effects are playing an important role with respect to safety and environmental sustainability of existing and future aircraft. Especially, the flight at a Mach number $Ma_\infty \approx 1$ offers challenges within the aeroelastic analysis since the established potential flow theory-based approaches are not suited to capture the nonlinear

* Research Engineer, Institute of Aerodynamics and Fluid Mechanics, maximilian.winter@aer.mw.tum.de
† Professor, Institute of Aerodynamics and Fluid Mechanics

characteristics of a transonic flow field. In contrast, computational fluid dynamics (CFD) methods based on the Euler or Reynolds-averaged Navier-Stokes (RANS) equations are able to reproduce the position and strength of shock waves, which have a crucial influence on the flow-induced load distribution [1]. However, a CFD-based multidisciplinary analysis increases the numerical cost substantially due to the large number of influence parameters (e.g., number of eigenmodes, free-stream Mach numbers, and incidence angles) in combination with the high effort for each individual simulation.

For this reason, the development of reduced-order models (ROMs) regarding aeroelastic applications is a research area of rising importance. The objective of ROMs is the reduction of the full-order problem to a more efficient and less complex system description under the premise that the essential characteristics of the underlying system are preserved. Within the present work, a ROM is considered as a mathematical model conditioned by high-fidelity CFD simulations. Recently, several ROM concepts have been published for aeroelastic applications. In the following, a brief description of the context-relevant approaches is given.

In the last decade, Lucia et al. [2] as well as Dowell and Hall [3] gave a comprehensive overview of several reduced-order techniques; e.g., harmonic balance (HB), Volterra theory, and proper orthogonal decomposition (POD), while showing their application to aeroelastic test cases. The latter method is a popular parameter reduction technique used by various authors within the aeroelasticity and fluid dynamics community, while the application examples vary from steady to unsteady decompositions of two- and three-dimensional flow fields (see Lucia et al. [4], Hall et al. [5], Willcox and Peraire [6], and Iuliano and Quagliarella [7] for instance). For reducing the system's degrees of freedom, several possibilities exist to incorporate the POD approach into time and frequency domain CFD solvers. Though, the focus in this work is on the utilization as a post-processing tool by means of the so-called snapshot method (see Sirovich [8]).

Other references suggest the use of linear system identification techniques to obtain an efficient aerodynamic model. A well-known example from this branch is based on the eigensystem realization algorithm (ERA) that is employed by Silva and Bartels [9] to construct a linear time-invariant state-space model. Moreover, some linear aerodynamic ROMs have been derived from the external dynamics approach, which is an established system identification concept [10]. Examples regarding these ROMs are the autoregressive moving average (ARMA) [11] and the autoregressive with exogenous input (ARX) method [12]. However, the aforementioned models are suited to capture only the linear dynamic characteristics around a nonlinear reference state.

Hence, various methods based on nonlinear system identification (NSI) principles have been developed concurrently in order to reproduce nonlinear dynamic effects. In 1997, Faller and Schreck [13] proposed a recurrent multi-layer-perceptron neural network (MLP-NN) for the identification of experimentally gathered aerodynamic coefficients. Subsequently, Marques and Anderson [14] used a multi-layer-based temporal neural network to predict unsteady aerodynamic forces in transonic flow. Consequently, Voitcu and Wong [15] demonstrated the suitability of neural networks for modeling the dynamic behavior of aeroelastic systems. Subsequently, Zhang et al. [16] and Winter and Breitsamter [17] employed radial basis function neural networks (RBF-NN) for the accurate modeling of unsteady aerodynamic force coefficients in transonic flow. Recently, Winter and Breitsamter [18] utilized local linear neuro-fuzzy models to construct an unsteady aerodynamic ROM that is valid across a range of Mach numbers including the subsonic and transonic flight regime.

Moreover, some combinations of the system identification methods with the POD-based approaches have been published. Within an aeroelastic optimization framework, Park et al. [19] employed the POD and a neural network for the ROM construction with respect to static flow fields. Recently, a successful combination of Zhang's RBF-based nonlinear system identification approach with the POD had been proposed by Lindhorst et al. [20].

In the present paper, a surrogate modeling approach comparable to the method of Lindhorst et al. is followed since neural networks and POD are conjointly used for unsteady aerodynamic predictions. Here, the POD is applied to the discrete (unsteady) pressure coefficient distribution in order to extract the dominant flow modes. The POD coefficients needed to reconstruct the training solution are obtained by solving a least-squares optimization problem. Then, the local linear neuro-fuzzy model is utilized to train the dynamic relationship between the structural excitation and the corresponding POD coefficients. The presented approach is applied to the LANN wing [21] undergoing a pitching motion in order to validate and demonstrate the method. For this purpose, the ROM results are compared with the corresponding time-accurate CFD solutions in the transonic flow regime.

2. THEORY AND NUMERICAL METHODS

In this section, the numerical approach of the surrogate-based ROM is discussed. Therefore, the parameter reduction method (POD) is introduced while the focus is on an application-oriented presentation. Subsequently, the local linear neuro-fuzzy approach is addressed. Finally, the employed inviscid CFD solver AER-Eu as well as the excitation strategy are discussed briefly.

2.1 Proper Orthogonal Decomposition (POD)

The POD is a mathematical procedure used to decompose a large multi-dimensional data-set into a much smaller number of representative modes yielding a compact system description.
Here, the so-called POD snapshot method introduced by Sirovich [8] is used. In this context, the surface pressure coefficients (C_p) at each time step are arranged as a vector, which is considered as the snapshot $\boldsymbol{W}_i$. Assuming that an available unsteady training data-set consists of N_{Trn} samples, the full-order snapshot matrix $\boldsymbol{Y}$ can be written as

$$\boldsymbol{Y} = \left[\widehat{\boldsymbol{W}}_1, \widehat{\boldsymbol{W}}_2, \dots, \widehat{\boldsymbol{W}}_{N_{Trn}}\right] \in \mathbb{R}^{S \times N_{Trn}} \tag{1a}$$

$$\widehat{\boldsymbol{W}}_i = \boldsymbol{W}_i - \boldsymbol{A}, \qquad \boldsymbol{A} = \frac{1}{N_{Trn}} \sum_{i=1}^{N_{Trn}} \boldsymbol{W}_i \ . \tag{1b}$$

In Eq. (1), S denotes the number of surface elements, while $\widehat{\boldsymbol{W}}_i$ represents the i-th centered snapshot vector. Moreover, $\boldsymbol{A} \in \mathbb{R}^S$ contains the time-averaged pressure coefficients. The aim of the POD is to find $M \ll N_{Trn}$ orthogonal basis vectors such that they approximate the snapshot matrix $\boldsymbol{Y}$ optimally in the least-squares sense. Therefore, the singular value decomposition (SVD) with respect to the snapshot matrix is calculated [7], leading to

$$\boldsymbol{Y} = \boldsymbol{U}\boldsymbol{\Sigma}\boldsymbol{V}^T = \boldsymbol{U} \begin{pmatrix} \sigma_1 & \cdots & 0 \\ \vdots & \ddots & \vdots \\ 0 & \cdots & \sigma_{N_{Trn}} \\ 0 & \cdots & 0 \end{pmatrix} \boldsymbol{V}^T. \tag{2}$$

As a result of the SVD, Eq. (2) contains the unitary matrix $\boldsymbol{U} \in \mathbb{R}^{S \times S}$ and the rectangular diagonal matrix $\boldsymbol{\Sigma} \in \mathbb{R}^{S \times N_{Trn}}$, while the first N_{Trn} column vectors of $\boldsymbol{U}$ correspond to the full set of possible POD modes. Therefore, using the N_{Trn} basis vectors it is possible to reconstruct the snapshot matrix exactly. However, since the singular values σ_i are ordered such that $\sigma_1 \geq \sigma_2 \geq \cdots \geq \sigma_{N_{Trn}} \geq 0$, the singular values with larger subscripts become comparatively small for practical applications. As the singular value is a measure of the mode's relative significance, higher modes ($M+1, \dots, N_{Trn}$) can be discarded in order to reduce the number of degrees of freedom, while maintaining the dominant system characteristics. For an adequate selection of the number of relevant modes M, the relative information content (RIC) criterion is evaluated:

$$RIC = \frac{\sum_{i=1}^{M} \sigma_i}{\sum_{j=1}^{N_{Trn}} \sigma_j} \geq \varepsilon \tag{3}$$

In Eq. (3), ε is a user-defined energy contribution threshold which should be set to 99% according to [7]. The resulting POD modes $\boldsymbol{\phi} \in \mathbb{R}^{S \times M}$ are determined as a subset of the matrix $\boldsymbol{U}$. Thus, the full-order problem can be approximated by the relation

$$\boldsymbol{W}(t) \cong \boldsymbol{A} + \sum_{i=1}^{M} b_i(t)\, \boldsymbol{\phi}_i \,, \tag{4}$$

considering the M dominant basis vectors. In order to construct a ROM, the time-dependent POD coefficients $b_i(t)$ have to be determined based on the training data-set. For this purpose, a least-squares optimization is performed with respect to the snapshot matrix $\boldsymbol{Y}$ and the POD modes $\boldsymbol{\phi}$. In this way, the matrix of POD coefficients ($\boldsymbol{B} = [\boldsymbol{b}(t_1), \dots, \boldsymbol{b}(t_{N_{Trn}})] \in \mathbb{R}^{M \times N_{Trn}}$) is obtained. For a given training data-set, the structural excitation and the corresponding POD coefficient time series are known quantities and can, therefore, serve as the respective input and output for a system identification-based model.

2.2 Nonlinear System Identification Approach based on Local Linear Neuro-Fuzzy Models

It is well-known from system identification theory [10, 22] that the output of a discrete-time dynamic system can be approximated as a function of current excitation inputs in combination with a certain number of previous inputs and previous system responses (feedback). This principle, also known as the external dynamics approach, can be combined either with a linear or a nonlinear function approximation method, leading to the auto-regressive with exogenous input (ARX) or the nonlinear auto-regressive with exogenous input (NARX) model architecture, respectively. The aforementioned methodologies refer to the fact that the system outputs known from the provided training data-set are used for calibrating the unknown model parameters. Hence, the feedback of the output quantities has to be taken into account only for application/generalization of the model and not within the training process. When using the ROM for simulating the aerodynamic system, the previous model outputs are fed back by means of the input vector.
In the present work, the input is defined to be the amplitude pitch angle $\hat{\alpha}(k)$, whereas the outputs are the respective time-domain POD coefficients $\tilde{b}_i(k)$ (with $i = 1, 2, \dots, M$). Thus, the knowledge about a finite time-series of those quantities is sufficient to yield a one-step prediction, as depicted in Fig. 1. Defining that k is the current discrete-time increment ($t_{k+1} = t_k + \Delta t$), the relationship for the training procedure can be expressed as:

$$\tilde{b}_i(k) = \mathcal{N}\left(\underbrace{\begin{pmatrix} \hat{\alpha}(k) \\ \hat{\alpha}(k-1) \\ \vdots \\ \hat{\alpha}(k-m) \end{pmatrix}, \begin{pmatrix} b_i(k-1) \\ b_i(k-2) \\ \vdots \\ b_i(k-n) \end{pmatrix}}_{\boldsymbol{u}_i \in \mathbb{R}^p} \right) \tag{5}$$

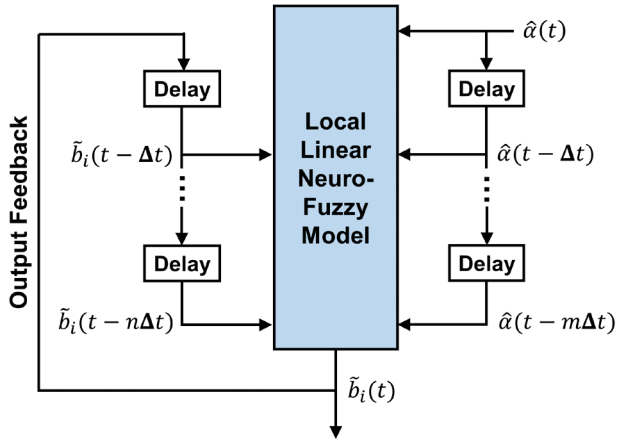

Fig. 1: Schematic of the external dynamics approach (application/feedback mode) for approximating POD coefficients as a function of the structural excitation (here: amplitude angle of attack).

The maximum dynamic delay-orders introduced in Eq. (5) are $m \in \mathbb{N}$ for the inputs and $n \in \mathbb{N}$ for the outputs, respectively. Because the a priori unknown function $\mathcal{N}$ is typically of nonlinear nature, an adequate functional mapping has to be realized in order to model the underlying aerodynamic characteristics.
For this purpose, the local linear neuro-fuzzy model from the domain of artificial neural networks (ANNs) has been selected in this work [22]. This mathematical framework can be utilized to approximate a nonlinear multi-dimensional function based on given training data. Therefore, various local linear models (LLMs) that are valid in certain regimes of the model input space are blended to yield the nonlinear relationship. The assignment of each LLM to the respective input space is thereby realized via fuzzy validity functions. According to Nelles [22], the basis function formulation for a local linear neuro-fuzzy model with N_{LLM} local linear sub-models can be generalized to:

$$\tilde{b}_i = \sum_{j=1}^{N_{LLM}} \left[w_{j0} + w_{j1} u_{1,i} + \cdots + w_{jp} u_{p,i} \right] \cdot \Psi_j(\boldsymbol{u}_i) \quad (6)$$

In Eq. (6), the coefficients w_{xy} represent the linear model parameters spanning a hyperplane in the p-dimensional input space, while $u_{x,y}$ denotes the x-th element of the network input vector related to the output $\tilde{b}_y$ (see also Eq. 5). Moreover, Ψ_j refers to the fuzzy validity function that is linked with the j-th LLM and is composed of (normalized) Gaussian functions evaluated with the Euclidean distance from the input vector to the center of the neuron. In this context, the employed validity functions containing the respective centers and widths c_{xy} and σ_{xy} of each LLM are described by the relations

$$\Psi_j(\boldsymbol{u}_i) = \frac{\mu_j(\boldsymbol{u}_i)}{\sum_{k=1}^{N_{LLM}} \mu_k(\boldsymbol{u}_i)}, \quad (7a)$$

$$\mu_j(\boldsymbol{u}_i) = \exp\left[-\frac{1}{2} \left(\frac{(u_{1,i} - c_{j1})^2}{\sigma_{j1}^2} + \cdots + \frac{(u_{p,i} - c_{jp})^2}{\sigma_{jp}^2} \right) \right]. \quad (7b)$$

Equations (6) and (7) define the general structure of the neural network. Though, various unknowns have to be determined to obtain an adequate model. Those unknowns are the weights w_{xy}, centers c_{xy}, and basis function widths σ_{xy}. For that purpose, a set of training and validation data has to be exploited, containing the information about the inputs $\hat{\alpha}(k)$ and the outputs $b_i(k)$ of the investigated system for a series of discrete time steps. Assuming that valid data-sets are available, the local linear model tree algorithm (LOLIMOT, [22]) can be applied to train the unknown parameters of the local linear neuro-fuzzy model.
LOLIMOT is an iterative model construction algorithm that starts from estimating a global linear model and proceeds by dividing the input space into axis-orthogonal partitions. This strategy leads to an iteratively expanding model structure, while the input space is refined only in regions with distinct nonlinearities. Besides the numerical efficiency due to the use of sophisticated and fast linear optimization techniques, the LOLIMOT algorithm offers several advantages for modeling dynamic systems, e.g., the linear extrapolation behavior. More information about the training procedure can be found in Nelles [22] and Winter and Breitsamter [18].

2.3 Computational Fluid Dynamics – AER-Eu

In the present work, the Euler solver AER-Eu is used to provide the ROM with high-quality training data for the steady and unsteady aerodynamics. Moreover, AER-Eu is used for intermethod comparisons in order to assess the accuracy of the surrogate modeling approach. In this research, the purpose of the ROM is to reproduce the underlying CFD system, which is considered as the reference.
AER-Eu solves the Euler equations in conservation form by utilizing a shock-capturing finite-volume method for structured multi-block grids [23]. The spatial discretization is realized by Roe's flux-difference splitting [24], while the MUSCL extrapolation (from monotonic upstream scheme for conservation laws) is employed in order to retain the total variation diminishing (TVD) property. The temporal integration is performed with the dual-time stepping scheme, whereas the embedded pseudo-time solution is carried out using the lower-upper symmetric successive overrelaxation. Furthermore, a deforming mesh approach had been implemented. In this context, a user-defined time law can be prescribed to interpolate between a reference grid and various amplitude grids [25]. For further information, refer to [23, 26-28].

2.4 Excitation and Training Data Acquisition

Regarding linear system identification tasks, the impulse or step excitation involving one distinct amplitude is sufficient to realize a precise and stable model [10, 22]. However, the NSI approach requires more information about the underlying system in order to train the nonlinear ROM. Hence, the design of an adequate excitation signal is a challenging task. The signal has to excite the representative characteristics (amplitudes and frequencies) of the aerodynamic system. Concurrently, the generation of the training data-set must not be too computationally demanding to exploit the ROM advantages. Various excitation strategies and theories are given in the literature to fulfill these requirements. Here, the amplitude-modulated pseudo-random binary signal (APRBS, see [22, 17]) is chosen for the forced-motion structural excitation. This signal (schematically shown in Fig. 2) can be generated from the frequently used pseudo-random binary signal (PRBS) by assigning random amplitudes to each plateau. The main advantages of utilizing the APRBS are the large spectrum of excited frequencies and amplitudes and the high information content per signal length, which limits the computational cost.

3. AERODYNAMIC SURROGATE MODEL

In this section, the theoretical approaches described beforehand are combined in order to obtain a surrogate model that is capable of evaluating the unsteady aerodynamic pressure coefficient fluctuations with respect to structural excitations. Based on the schematic presented in Fig. 2, an application-oriented overview of the ROM procedure is given.

Since the ROM approach is based on system identification principles, the input/output model parameters must be trained before a simulation can be conducted. For this purpose, a set of training and validation data representing the underlying system must be provided. It is important to emphasize that only those structural amplitudes and frequencies that have been excited by the training data can be reproduced adequately by the ROM.

Hence, steady-flow solutions are computed using the CFD solver AER-Eu for a fixed incidence angle α_0 and Mach number Ma_∞. Subsequently, unsteady CFD solutions are generated with respect to the chosen free-stream conditions. For general applications, an APRBS is assigned to each structural coordinate q_i as depicted in Fig. 2. In the following, only a pitching motion $q_1(\tau) \rightarrow \hat{\alpha}(\tau)$ is considered. Therefore, a single APRBS is imposed to the instantaneous $\hat{\alpha}$ variation. Otherwise, the deformed geometry is formed by a superposition of all structural modes multiplied by the respective APRBS values. The result of the unsteady AER-Eu simulation is a time-series of C_p at each surface panel caused by the prescribed motion. It is important to emphasize that nonlinear aerodynamic phenomena such as moving shock-waves are taken into account using the time-accurate AER-Eu solver. Hence, their effect is incorporated in the surface pressure distribution.

Once the unsteady result is available, the POD snapshot matrix can be constructed, whereas the mean pressure field is obtained by applying Eq. (1b). The SVD in combination with a subsequent least-squares optimization yields the M most relevant POD modes and the POD coefficients corresponding to the training samples.

Thus, combining the structural inputs (APRBS) with

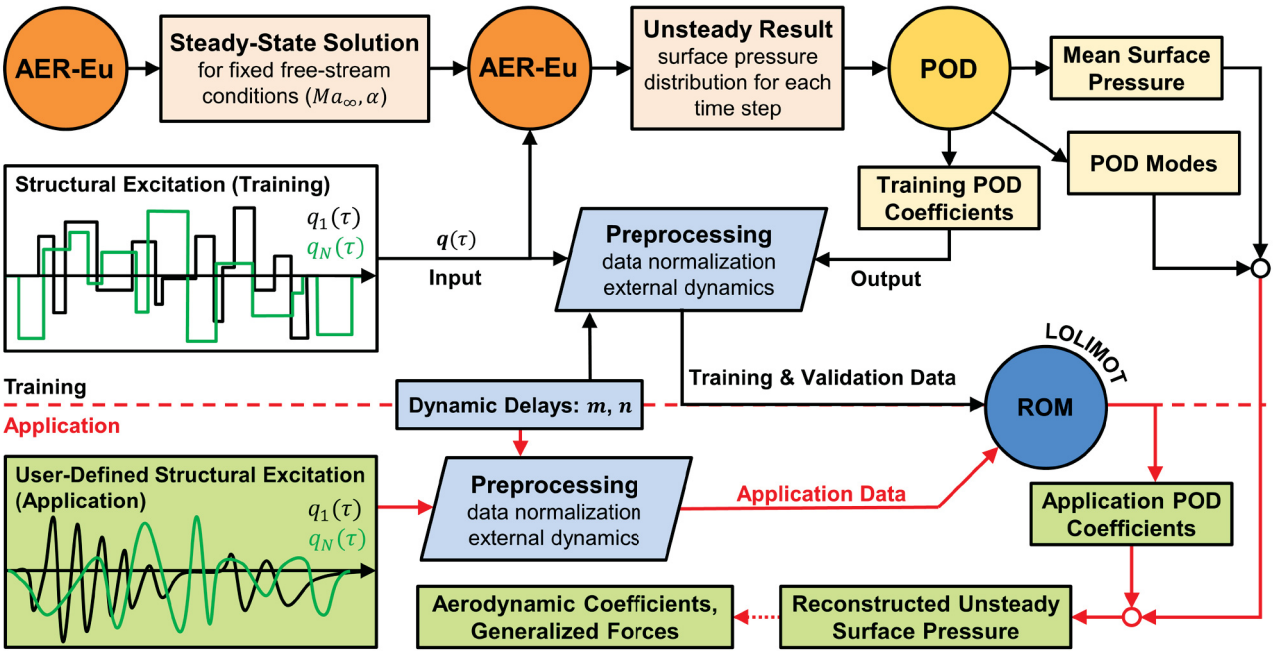

Fig. 2: Process chart of the surrogate modeling approach based on POD and neuro-fuzzy models.

the CFD-based POD coefficient time series, the merged data-set is used to calibrate the local linear neuro-fuzzy model. Before the LOLIMOT model construction algorithm can be applied, some preprocessing steps are required. Firstly, the data should be normalized in order to improve the numerical robustness of the training procedure. Secondly, the maximum dynamic delays (m, n) must be defined by the user to arrange the data according to the external dynamics principle. Because of the iterative nature of finding optimal delay parameters, a further adjustment of the respective quantities may be necessary.

After the preprocessing step, the data can be utilized to train the unknown parameters of the local linear neuro-fuzzy model by applying the LOLIMOT algorithm. For this purpose, the available CFD-based data is randomly segmented, while typically around 70% of the samples are used for the training. The remaining data is exploited for validation purposes in order to realize a stable and accurate model.

If the model error evaluation yields acceptable results, the ROM can be used for time-marching aerodynamic simulations by performing multiple one-step predictions. Therefore, arbitrary structural excitation signals can be preprocessed and fed into the neuro-fuzzy model as depicted in Fig. 2. However, the excitation amplitudes should be covered by the training data to obtain adequate results. In contrast to the training process, the model outputs (estimated POD coefficients) have to be fed back to the neural network input vector within each iteration. Moreover, the nondimensional discrete time step size $\Delta\tau$ embedded in the training data-set is fixed for the model and has to be utilized for all intended simulations.

Once the neural-network-based POD coefficients caused by the user-defined excitation (application mode) have been obtained, the data can be used to reconstruct the surface pressure distribution by means of the determined POD mode shapes and the mean flow state. If not only the discrete pressure coefficient values are sought-after but also integral quantities, the aerodynamic coefficients or generalized aerodynamic forces can be easily calculated using the available data. Due to these properties, the constructed ROM can be coupled with a structural and/or flight mechanics solver in order to realize a highly-efficient multi-physics framework.

4. RESULTS

For validation and demonstration purposes, the surrogate modeling process is applied to the LANN wing configuration undergoing a pitching motion at transonic flow conditions. The objective of this investigation is to analyze and compare the ROM results with corresponding AER-Eu simulations. In this context, the surface pressure distribution as well as integral aerodynamic coefficients are considered for comparisons. Additionally, some considerations about the numerical efficiency are presented.

4.1 LANN Wing Configuration

The LANN wing [21] is a well-known three-dimensional test configuration within the unsteady aerodynamics community since it offers a challenging λ-shock system on the suction side of the wing at a Mach number of 0.82 and a steady/mean angle of attack of 0.6 deg (see Fig. 3). The aforementioned free-stream conditions belong to the AGARD CT5 test case and have been selected for this investigation. According to Zwaan [21], the pitching axis is placed at 62.1% of the root chord ($c_{root} = c_{ref} = 1.0\,m$). The amplitude pitch angle $\hat{\alpha}$ considered in the CT5 case (0.25 deg), however, is increased to 2.0 deg in order to obtain a stronger nonlinear behavior induced by the larger shock motion. Therefore, the considered setup is well-suited to assess the fidelity of the nonlinear surrogate model. Because this paper presents preliminary results, only inviscid flow was taken into account, although viscous effects have a non-negligible impact on the aerodynamic characteristics. For the consideration of viscous flow, the Euler-CFD solver must be replaced by a RANS solver, which remains a topic for future research.

The employed reference CFD grid is discretized by 368,640 cells in a two-block C-H topology using the commercial ICEM-CFD software [30]. A grid-sensitivity study was carried out to ensure the independence of the solution from the spatial discretization. In Fig. 3, the CFD grid is visualized along with the steady-state pressure coefficient distribution for the free-stream parameters related to the AGARD CT5 case. Moreover, the deformed CFD grid (pitch deflection) is generated via a rigid body rotation of the grid points.

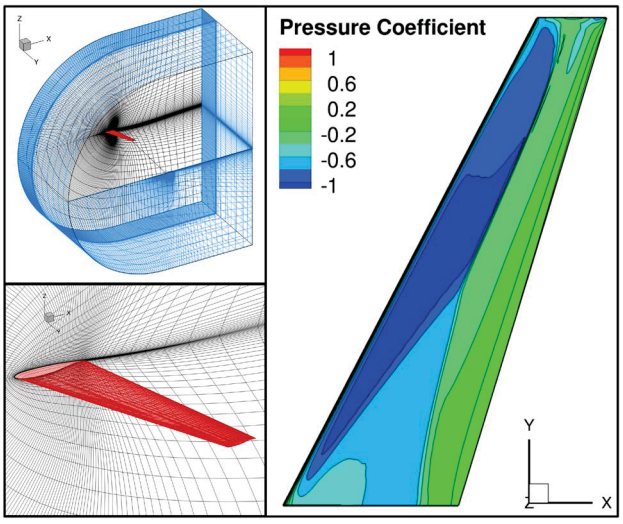

Fig. 3: Left: Topology and detailed wing discretization of the structured reference CFD grid. Right: steady-state C_p contours of the upper LANN wing surface at $Ma_\infty = 0.82$ and $\alpha_0 = 0.6\,deg$ (AER-Eu).

4.2 Surrogate Model Training

Based on the steady-state AER-Eu solution, an unsteady forced-motion CFD simulation was performed yielding the ROM training data. For this purpose, an APRBS excitation with respect to $\hat{\alpha}$ was generated in the range of -2 deg and 2 deg in order to enforce a quasi-random pitch angle variation (see Fig. 4). Moreover, a nondimensional time step size of $\Delta\tau = \Delta t/\left(\sqrt{\rho_\infty/p_\infty}\cdot 1\,m\right) = 0.3$ has been defined, leading to the displayed nondimensional time interval from 0 to 660 for the chosen 2201 training samples.

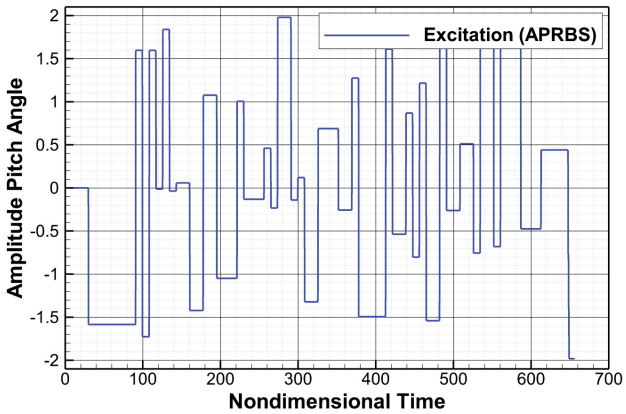

Fig. 4: APRBS excitation with respect to $\hat{\alpha}$. The pitch angle α is given as $\alpha(\tau) = \alpha_0 + \hat{\alpha}(\tau)$.

Based on the unsteady CFD data-set, the POD procedure was carried out to obtain the POD modes as well as the corresponding POD coefficients. To achieve a RIC value larger than 99%, $M = 274$ modes have been selected for the investigated case. Figure 5 shows exemplarily the first three POD coefficients caused by the prescribed excitation. Moreover, the first five POD modes as well as the calculated mean C_p distribution are depicted in Fig. 7.

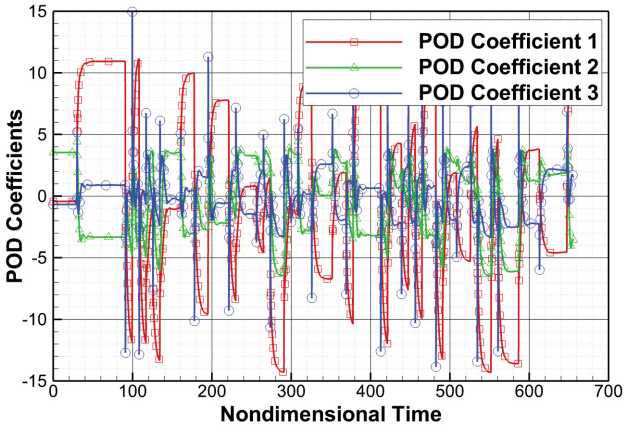

Fig. 5: Response of the first three POD coefficients due to the APRBS excitation displayed in Fig. 4 (LANN wing, $Ma_\infty = 0.82$, $\alpha_0 = 0.6\,deg$).

Hence, a 274 x 2201 matrix is obtained for the POD coefficient response, while the model input is characterized by the amplitude pitch angle time series (matrix containing 1 x 2201 elements). Next, the previously obtained data-sets have been preprocessed according to the workflow presented in Fig. 2. Therefore, the dynamic delay orders for the external dynamics approach were fixed to $m = n = 5$ for the respective model inputs and outputs.
Then, the local linear neuro-fuzzy model was trained using the LOLIMOT algorithm, whereas the maximum number of LLMs was limited to 10. After concluding the data acquisition and model construction process, the ROM is considered fixed in the following and, therefore, can be used for unsteady aerodynamic computations.

4.3 ROM Application and Computational Effort

In the following, the simulation of an arbitrary structural excitation for the same underlying system is studied. In this context, the system is assumed identical, if Ma_∞, α_0, and $\Delta\tau$ remain unchanged; i.e., in accordance with the initial training data. The surrogate model is demonstrated by calculating the time-domain response due to harmonic pitch angle oscillations ($-2\,deg \le \hat{\alpha} \le 2\,deg$). In order to achieve load periodicity, three oscillation cycles are computed with the constructed ROM and the AER-Eu solver. For the latter method, each cycle is resolved with 100 nondimensional time steps. In contrast, the ROM is applied using a constant time step size ($\Delta\tau = 0.3$), leading to a frequency-dependent cycle discretization. Here, the results for two reduced frequencies ($k_{red} = c_{root}\cdot 2\pi f/U_\infty = [0.1, 0.5]$) are presented in order to evaluate the effect of the frequency on the ROM performance.
Thus, the user-defined time law related to $\hat{\alpha}$ is fed into the ROM, resulting in the corresponding time-discrete POD coefficients. In Fig. 6, the output of the neuro-fuzzy model is shown for the harmonic excitation with $k_{red} = 0.1$. It is apparent that for the second POD coefficient a strong nonlinear dependency with respect to the sine input is obtained, justifying the use of a nonlinear function approximation approach.

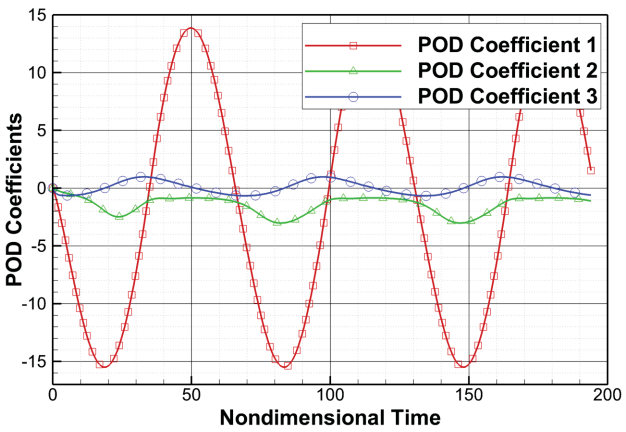

Fig. 6: First three ROM-based POD coefficients due to a harmonic excitation with $k_{red} = 0.1$ (LANN wing, $Ma_\infty = 0.82$, $\alpha_0 = 0.6\,deg$).

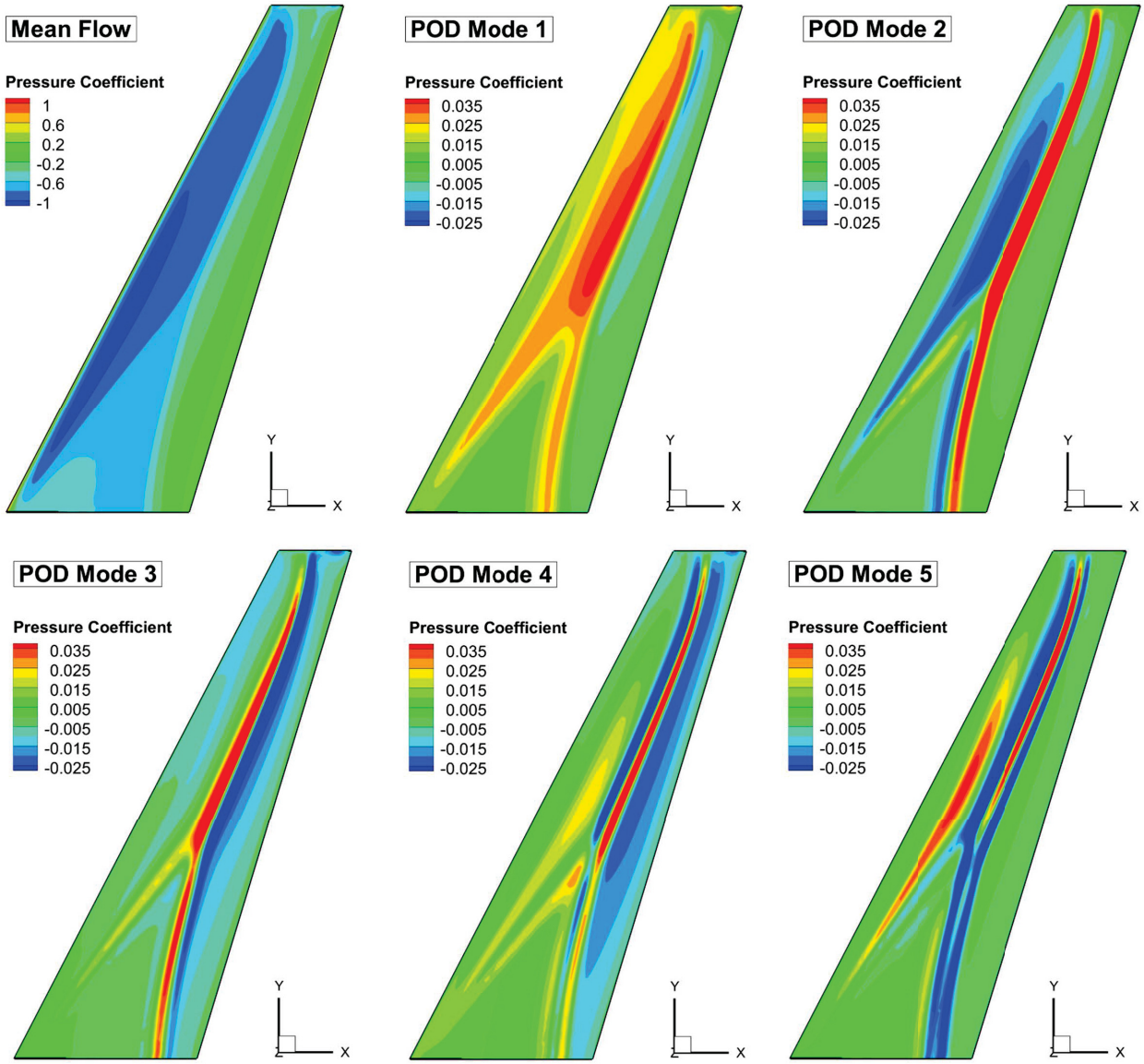

Fig. 7: Mean surface pressure coefficient distribution and the first five POD modes extracted from the unsteady CFD data samples. The upper side of the LANN wing is shown. $Ma_\infty = 0.82$ and $\alpha_0 = 0.6\,deg$ (AER-Eu).

Using the newly generated POD coefficients in combination with the stored POD modes (partly depicted in Fig. 7), the unknown pressure coefficients for all surface elements and time steps are obtained via weighted superposition (see Eq. (4)). Introducing the nondimensional period T with respect to the third excitation cycle, the ROM results can be compared to the corresponding full-order CFD simulation. In Fig. 8, the C_p distribution originating from the surrogate approach is visualized in contrast to the AER-Eu results ($k_{red} = 0.5$). In this context, four equidistant time steps within the third period are presented. Although the shock is not as sharp for the ROM as for the CFD result, the contour plots exhibit a generally good agreement. Some minor artifacts and unphysical oscillations exist within the pressure distribution. However, the solution quality regarding the structural loading seems to be sufficient for fast multidisciplinary predictions.

A further study focuses on the local accuracy of the ROM approach. For that purpose, a cross-section at 32.5% of the half-span measured from the wing root is considered. In Fig. 9, the chordwise C_p characteristics are plotted for a harmonic excitation with $k_{red} = 0.1$ and four equidistant time steps of the third cycle. In general, a good conformity is observed, which holds especially true for the pressure side. Regarding the suction side, the position of the shock is captured to some extent; i.e., the mean position of the pressure drop is in agreement with the reference. However, the shock intensity is distinctly reduced in comparison to the CFD result. This also affects adjacent parts of the solution and deteriorates the local accuracy. The described phenomenon, that discontinuities such as shocks are not well captured using the POD's linear superposition principle, had been also noted by several authors with respect to static approximation problems [4, 7].

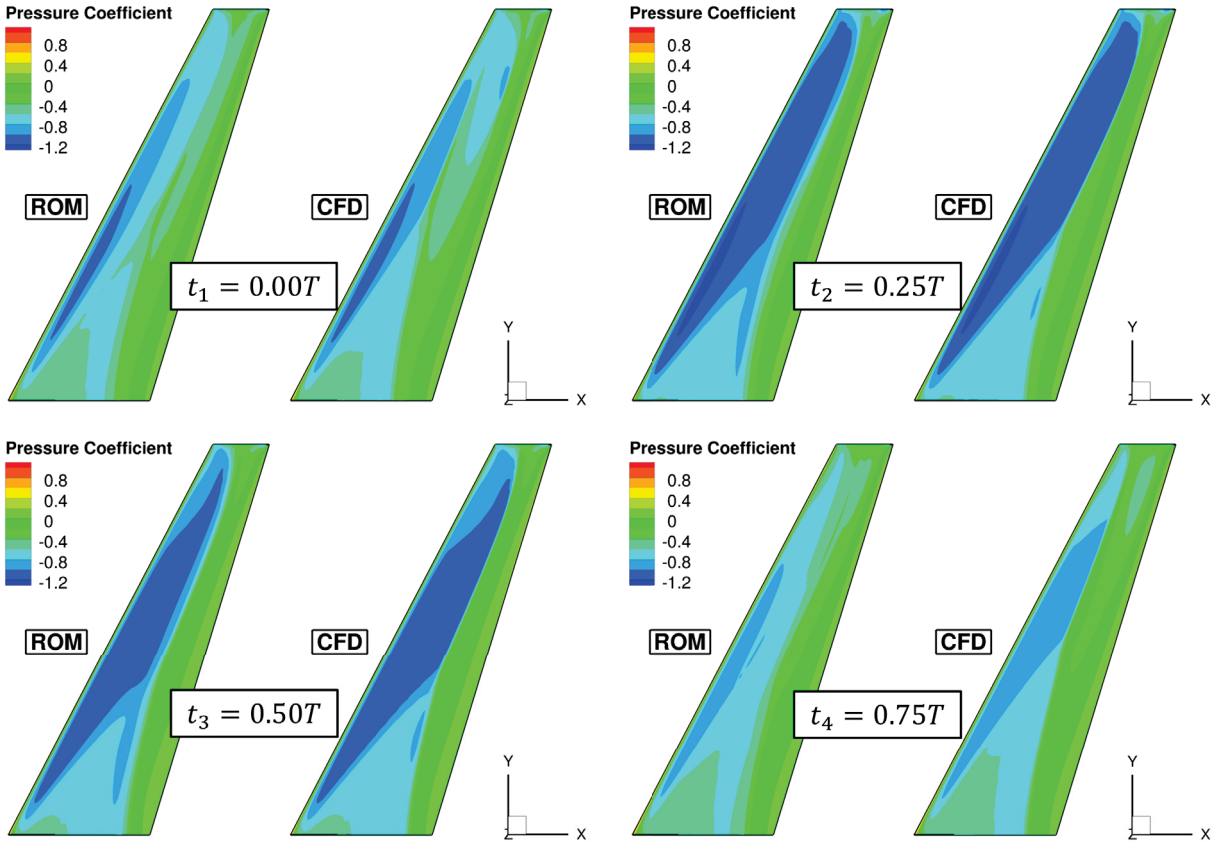

Fig. 8: Pressure coefficient distribution induced by a harmonic pitching motion with a reduced frequency of 0.5 (third cycle). The upper side of the LANN wing is shown. $Ma_\infty = 0.82$ and $\alpha_0 = 0.6\,deg$ (ROM and AER-Eu).

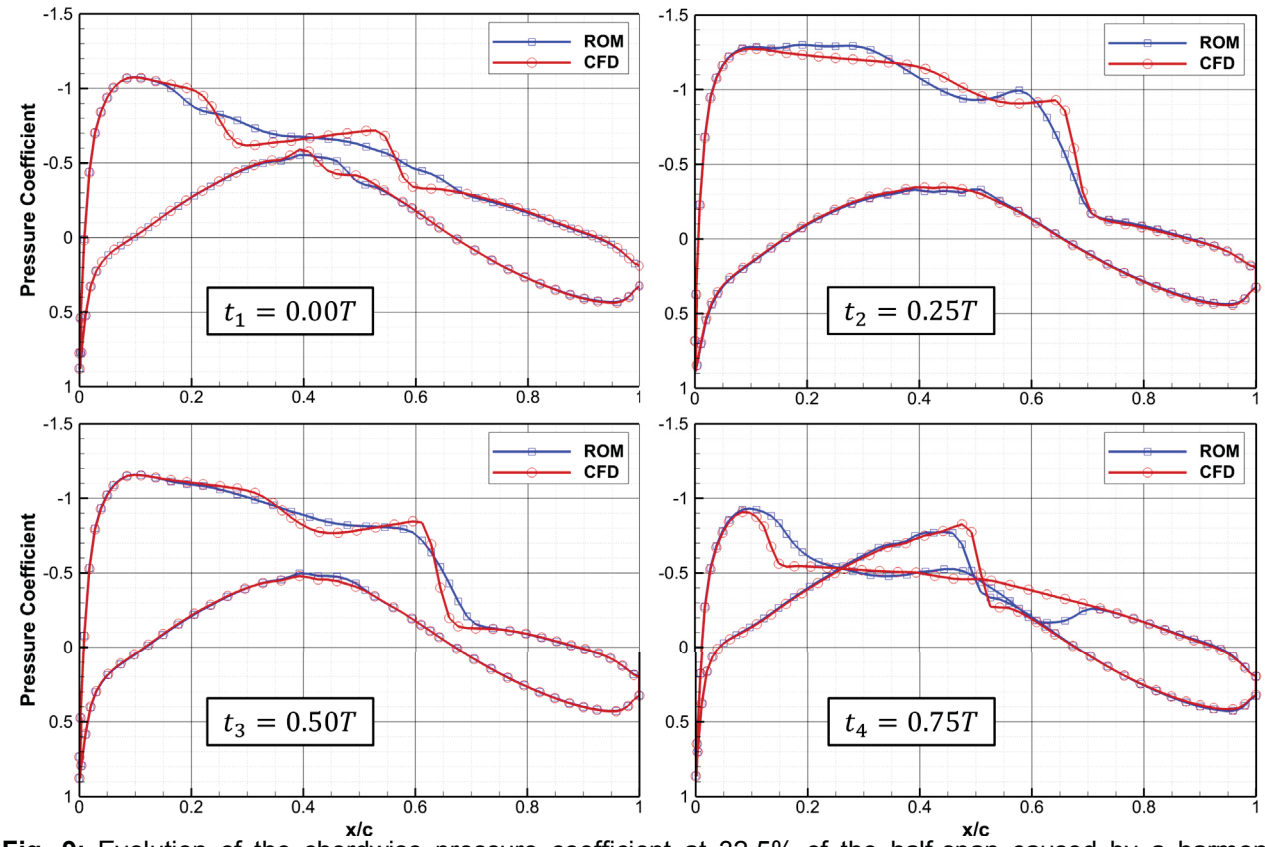

Fig. 9: Evolution of the chordwise pressure coefficient at 32.5% of the half-span caused by a harmonic excitation with $k_{red} = 0.1$ (third cycle). LANN wing, $Ma_\infty = 0.82$ and $\alpha_0 = 0.6\,deg$ (ROM and AER-Eu).

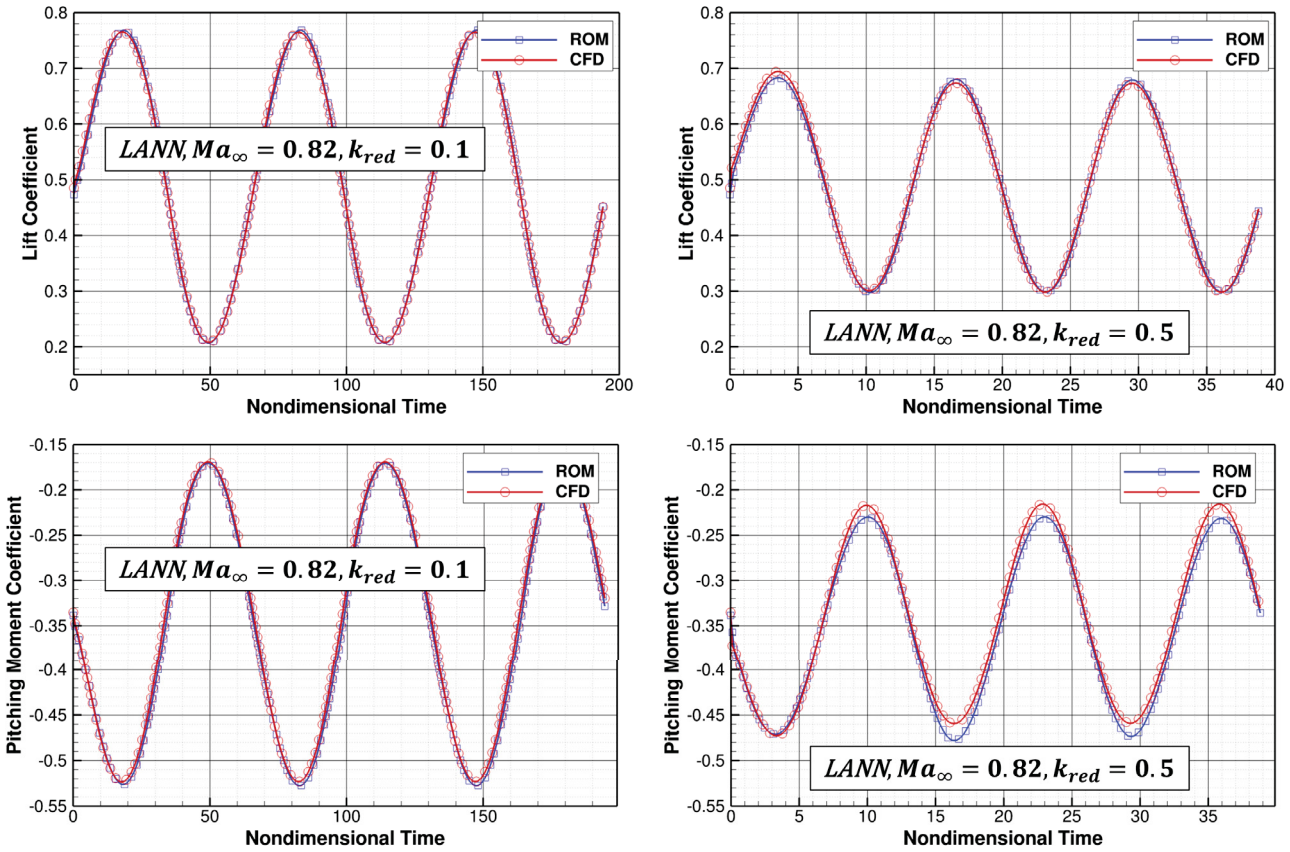

Fig. 10: Time-varying lift and pitching moment coefficients evaluated for the surrogate model and the reference CFD solver results (both considered reduced frequency cases). LANN wing, $Ma_\infty = 0.82$ and $\alpha_0 = 0.6\ deg$.

Finally, the lift and pitching moment coefficients have been calculated from the respective surface pressure distributions in order to discuss the solution quality with respect to integral quantities. The pitching moment was thereby related to the quarter chord. In Fig. 10, the results are depicted for both considered reduced frequencies. Although some local deviations exist for the ROM solution with respect to the CFD reference (refer to the discussion above), the diagrams indicate a very good agreement for the integral forces (C_L). If the local influence becomes important (as for the pitching moment evaluation), the discrepancies become larger. The overall solution quality, however, is good for the integral results.

All presented computations have been performed on a single Intel Xeon 2.3 GHz processor. In this context, the computational effort of a ROM simulation was less than a second. However, the training data generation (APRBS-CFD simulation; here: 32.2 CPU hours) as well as the POD application and training cost (0.1 + 0.2 CPU hours) must be considered for a total cost estimation as well. Therefore, about 33 CPU hours were needed for constructing the surrogate model. In comparison, the AER-Eu computation for the harmonic excitation with two distinct frequencies took about 10.2 CPU hours. Thus, with an increased number of intended simulations, the computational advantage is increased. This is of particular interest for computationally intensive multidisciplinary simulations, i.e., fluid-structure-interaction problems.

5. CONCLUSIONS

In the present paper, an unsteady aerodynamic surrogate modeling approach was presented that is based on the proper orthogonal decomposition method combined with a local linear neuro-fuzzy model. Thereby, the first approach realizes a substantial parameter reduction, whereas the neural network is applied in terms of a nonlinear system identification. Starting from the theoretical fundamentals, the reduced-order model was demonstrated for pressure coefficient predictions regarding the entire surface of the LANN wing undergoing a pitching motion. Moreover, the method is generally valid for other physical quantities and could be also employed for modeling the whole three-dimensional flow domain. It was shown that the approach can adequately predict the dominant unsteady aerodynamic characteristics. However, the shock resolution, especially for higher excitation amplitudes, is still challenging. This can be interpreted as a limitation of the utilized linear parameter reduction method. Nevertheless, the resulting highly-efficient model linked with an overall satisfying solution accuracy is interesting for multidisciplinary research fields, i.e., aeroelasticity, load estimation, and optimization.

ACKNOWLEDGMENTS

The authors would like to thank the Bavarian Research Foundation (Bayerische Forschungs-stiftung, BFS) for the funding of the project ROM-Aer (AZ 1050-12).

REFERENCES

[1] O. O. Bendiksen, "Review of Unsteady Transonic Aerodynamics: Theory and Applications," *Progress in Aerospace Sciences, Vol. 47,* pp. 135-167, 2011.

[2] D. J. Lucia, P. S. Beran and W. A. Silva, "Reduced-Order Modeling: New Approaches for Computational Physics," *Progress in Aerospace Sciences, Vol. 40,* pp. 51-117, 2004.

[3] E. H. Dowell and K. C. Hall, "Modeling of Fluid-Structure Interaction," *Annual Review of Fluid Mechanics, Vol. 33,* pp. 445-490, 2001.

[4] D. J. Lucia, P. I. King and P. S. Beran, "Reduced-Order Modeling of a Two-Dimensional Flow," *Computers & Fluids, Vol. 32,* p. 917–938, 2003.

[5] K. C. Hall, J. P. Thomas and E. H. Dowell, "Proper Orthogonal Decomposition Technique for Transonic Unsteady Aerodynamic Flows," *AIAA Journal, Vol. 38, No. 10,* pp. 1853-1862, 2000.

[6] K. Willcox and J. Peraire, "Balanced Model Reduction via the Proper Orthogonal Decomposition," *AIAA Journal, Vol. 40, No. 11,* pp. 2323-2330, 2002.

[7] E. Iuliano and D. Quagliarella, "Proper Orthogonal Decomposition, Surrogate Modelling and Evolutionary Optimization in Aerodynamic Design," *Computers & Fluids, Vol. 84,* pp. 327-350, 2013.

[8] L. Sirovich, "Turbulence and the Dynamics of Coherent Structures. Part 1: Coherent Structures," *Quarterly of Applied Mathematics, Vol. 45, No. 3,* pp. 561-571, 1987.

[9] W. A. Silva and R. E. Bartels, "Development of Reduced-Order Models for Aeroelastic Analysis and Flutter Prediction using the CFL3Dv6.0 Code," *Journal of Fluids and Structures, Vol. 19,* pp. 729-745, 2004.

[10] L. Ljung, System Identification: Theory for the User, Prentice-Hall, Upper Saddle River, NJ, 1987.

[11] K. Won, H. M. Tsai, M. Sadeghi und F. Liu, „Non-Linear Impulse Methods for Aeroelastic Simulations," *23rd AIAA Applied Aerodynamics Conference, AIAA Paper 2005-4845,* June 2005.

[12] W. Zhang and Z. Ye, "Reduced-Order-Model-based Flutter Analysis at High Angle of Attack," *Journal of Aircraft, Vol. 44, No. 6,* pp. 2086-2089, 2007.

[13] W. E. Faller and S. J. Schreck, "Unsteady Fluid Mechanics Applications of Neural Networks," *Journal of Aircraft, Vol. 34, No. 1,* pp. 48-55, 1997.

[14] F. D. Marques and J. Anderson, "Identification and Prediction of Unsteady Transonic Aerodynamic Loads by Multi-Layer Functionals," *Journal of Fluids and Structures, Vol. 15,* pp. 83-106, 2001.

[15] O. Voitcu and Y. S. Wong, "Neural Network Approach for Nonlinear Aeroelastic Analysis," *Journal of Guidance, Control, and Dynamics, Vol. 26, No. 1,* pp. 99-105, 2003.

[16] W. Zhang, B. Wang, Z. Ye and J. Quan, "Efficient Method for Limit Cycle Flutter Analysis by Nonlinear Aerodynamic Reduced-Order Models," *AIAA Journal, Vol. 50, No. 5,* pp. 1019-1028, 2012.

[17] M. Winter and C. Breitsamter, "Reduced-Order Modeling of Unsteady Aerodynamic Loads using Radial Basis Function Neural Networks," *63rd Deutscher Luft- und Raumfahrtkongress, Augsburg, Germany, DGLR Paper 2014-340013,* September 2014.

[18] M. Winter and C. Breitsamter, "Nonlinear Reduced-Order Modeling of Unsteady Aerodynamic Loads based on Dynamic Local Linear Neuro-Fuzzy Models," *16th International Forum on Aeroelasticity and Structural Dynamics, St. Petersburg, Paper IFASD-2015-82,* July 2015.

[19] S. O. Park, K. H. Jun, S. M. Baek, M. H. Cho, K. J. Yee and D. H. Lee, "Reduced-Order Model with an Artificial Neural Network for Aerostructural Design Optimization," *Journal of Aircraft, Vol. 50, No. 4,* pp. 1106-1116, 2013.

[20] K. Lindhorst, M. C. Haupt and P. Horst, "Efficient Surrogate Modelling of Nonlinear Aerodynamics in Aerostructural Coupling Schemes," *AIAA Journal, Vol. 52, No. 9,* pp. 1952-1966, 2014.

[21] R. Zwaan, "LANN Wing Pitching Oscillation," *Compendium of Unsteady Aerodynamic Measurements, Addendum Nr. 1. Technical Report, AGARD ,* 1982.

[22] O. Nelles, Nonlinear System Identification - From Classical Approaches to Neural Networks and Fuzzy Models, Springer, Berlin Heidelberg, 2001.

[23] E. Kreiselmaier and B. Laschka, "Small Disturbance Euler Equations: Efficient and Accurate Tool for Unsteady Load Predictions," *Journal of Aircraft, Vol. 37, No. 5,* pp. 770-778, 2000.

[24] P. L. Roe, "Approximate Riemann Solvers, Parameter Vectors and Difference Schemes," *Journal of Computational Physics, Vol. 43, No. 2,* pp. 357-372, 1981.

[25] D. Fleischer and C. Breitsamter, "Efficient Computation of Unsteady Aerodynamic Loads Using Computational-Fluid-Dynamics Linearized Methods," *Journal of Aircraft, Vol. 50, No. 2,* pp. 425-440, 2013.

[26] C. Weishäupl and B. Laschka, "Small Disturbance Euler Simulations for Delta Wing Unsteady Flows due to Harmonic Oscillations," *Journal of Aircraft, Vol. 41, No. 4,* pp. 782-789, 2004.

[27] A. Pechloff and B. Laschka, "Small Disturbance Navier–Stokes Method: Efficient Tool for Predicting Unsteady Air Loads," *Journal of Aircraft, Vol. 43, No. 1,* pp. 17-29, 2006.

[28] A. Pechloff and B. Laschka, "Small Disturbance Navier-Stokes Computations for Low Aspect-Ratio Wing Pitching Oscillations," *Journal of Aircraft, Vol. 47, No. 3,* pp. 737-753, 2010.

[29] The MathWorks, "MATLAB 2013b: User Manual," Natick, MA, 2013.

[30] ANSYS ICEM CFD 14.5, "User Manual," ANSYS, Canonsburg, PA, 2014.